





## Article

# Application of *Lolium multiflorum* as an Efficient Raw Material in the Production of Adsorbent for Removal of Methylene Blue

Elenara Oliveira da Silva <sup>1</sup>, Alair Valério Filho <sup>2</sup>, Emanuelle Butato de Araujo <sup>3</sup>, Taís Douglas Andrade <sup>3</sup>, Maele Costa dos Santos <sup>3</sup>, Ricardo Zottis <sup>3</sup>, Gabriela Silveira da Rosa <sup>1,3,\*</sup> and André Ricardo Felkl de Almeida <sup>1,3</sup>

<sup>1</sup> Graduate Program in Engineering, Federal University of Pampa, Alegrete 97546-550, Brazil; elenara.silva@gmail.com (E.O.d.S.); andrealmeida@unipampa.edu.br (A.R.F.d.A.)

<sup>2</sup> Graduate Program in Materials Science and Engineering, Technology Development Center, Federal University of Pelotas, Pelotas 96010-610, Brazil; alaorvf@msn.com

<sup>3</sup> Chemical Engineering, Federal University of Pampa, Bagé 96413-172, Brazil; emanuellearaujob@gmail.com (E.B.d.A.); taisandrade0912@gmail.com (T.D.A.); maeledossantoseq@gmail.com (M.C.d.S.); ricardozottis.eq@gmail.com (R.Z.)

\* Correspondence: gabrielarosa@unipampa.edu.br

**Abstract:** In this study, ryegrass straw agricultural residue (*Lolium multiflorum* L.) was employed as an adsorbent material to remove methylene blue (MB) dye from aqueous solutions. Four adsorbents were produced using phosphoric acid and pyrolysis as activating agents. The samples were analyzed with TGA, FTIR, SEM, and XRD techniques. A rapid adsorption of the MB was obtained with the ryegrass treated with 40% H<sub>3</sub>PO<sub>4</sub>, reaching equilibrium in 2 min. Moreover, a maximum adsorption capacity of 80.79 mg g<sup>-1</sup> and a removal efficiency of 99% were achieved. The results demonstrate a good performance of adsorbents from ryegrass for removing dye contaminants, such as methylene blue, from the aqueous solutions.

**Keywords:** ryegrass; methylene blue; agricultural waste



**Citation:** da Silva, E.O.; Valério Filho, A.; de Araujo, E.B.; Andrade, T.D.; dos Santos, M.C.; Zottis, R.; da Rosa, G.S.; de Almeida, A.R.F. Application of *Lolium multiflorum* as an Efficient Raw Material in the Production of Adsorbent for Removal of Methylene Blue. *C* **2023**, *9*, 44. <https://doi.org/10.3390/c9020044>

Academic Editors: Sergey Mikhalovsky and Rosa Busquets

Received: 7 March 2023

Revised: 23 April 2023

Accepted: 24 April 2023

Published: 26 April 2023



**Copyright:** © 2023 by the authors. Licensee MDPI, Basel, Switzerland. This article is an open access article distributed under the terms and conditions of the Creative Commons Attribution (CC BY) license (<https://creativecommons.org/licenses/by/4.0/>).

## 1. Introduction

Environmental pollution has reached a level of potential threat not only due to the environmental problems observed in the last years but also due to the health of the entire population [1,2]. Currently, water pollution is considered one of the main factors that affect the environment, and textile dyes are known as the world's most significant source of water pollution contaminants due to their release into water resources [3]. During the dyeing process in textile industries, a large fraction of the dye does not react with the cellulose fibers; therefore, about 20% of all dye used is discarded in effluents [4]. These residues are composed of non-biodegradable and recalcitrant molecules [5]. Several studies have focused on the treatment of colored effluents contaminated with methylene blue (MB) cationic dye [6–9] due to their complex degradation mechanism and high toxicity. Human exposure to MB dye can cause numerous health issues, such as vomiting, cyanosis, jaundice, shock, and tissue necrosis [10]. In addition, when present in water bodies the MB hinders the penetration of light, decreasing oxygen levels and harming the entire aquatic ecosystem, which can generate several carcinogenic and mutagenic problems in this biota [11,12].

Numerous techniques regarding the treatment of textile wastewater have already been reported, such as physical oxidation, biological degradation, cavitation, photocatalytic oxidation, and adsorption [5]. Among them, adsorption has emerged as being an extremely effective technique in effluent treatment due to its simplicity and the high percentage of removal of contaminants [13]. Even with it being a considerably inexpensive process, the main restriction of using adsorption in the treatment of effluents is the cost of the production of the adsorbent [14–16]. Thus, studies have their main focus on the search for alternative adsorbent materials [17–23]. In this sense, the use of agricultural waste can

be an effective alternative due to its abundance and low cost. Thus, it is considered an eco-friendly and sustainable resource [24,25]. Accordingly, Chahm et al. [8] and Ma [26] produced adsorbents from the waste of *Rapanea ferruginea* using  $H_2SO_4$  and wheat straw using KOH and  $ZnCl_2$ , respectively.

The *Lolium multiflorum* L. (LM), commonly known as ryegrass, is mostly used in subtropical regions. However, the south of Brazil is responsible for producing 5 to 8 tons per hectare that has no destination nor use [27,28].

In a previous work carried out by part of our team, LM was treated with NaOH for the production of activated carbon. Furthermore, in the investigation regarding the adsorption of MB dye, the best result reached  $67 \text{ mg g}^{-1}$  of maximum adsorption capacity for the LM treated with NaOH [28]. However, due to the abundance of Ryegrass biomass, we believe that other forms of activation should be studied. Hence, this work aims to add value to the agricultural waste of LM, proposing a sustainable use of it as an adsorbent and a raw material for activated carbon production. The adsorbents were produced using  $H_3PO_4$  and pyrolysis as activating agents and were investigated through TGA, DRX, and BET. The adsorption of the MB dye was analyzed using the mathematical models of kinetic and isotherm.

## 2. Materials and Methods

### 2.1. Preparation and Characterization of the Adsorbents

The dried LM straw was kindly supplied by EMBRAPA. The collected material was ground (Marconi, model Croton) and sieved in an electromagnetic sieve shaker (Bertel, model 4830, Brazil) to obtain particles with a size  $<2 \text{ mm}$ .

The chemical activation of the adsorbents was performed in a 1:1 ratio ( $w/w$ ) of  $H_3PO_4$  and LM. The samples were impregnated with  $H_3PO_4$  solution at a concentration of 40% or 70% and then oven-dried (Nova Ética, model 109-1, Brazil) at  $105 \text{ }^\circ\text{C}$  for 24 h. To obtain the activated carbons, a pyrolysis of the chemically activated samples was carried out in a stainless-steel reactor at  $550 \text{ }^\circ\text{C}$  for 1 h (heating rate of  $3 \text{ }^\circ\text{C min}^{-1}$ ) under an  $N_2$  atmosphere. Finally, all samples were washed with a sodium hydroxide solution until reaching a neutral pH. Figure 1 describes the methods and conditions used to synthesize each adsorbent.



**Figure 1.** Description of the adsorbent materials produced.

LM, R-40, R-70, AC-40, and AC-70 samples were characterized by the particle size diameter ( $d_{ps}$ ), obtained by sieving with Tyler sieves 9 to 270. The real densities ( $\rho_r$ ) were obtained by a helium gas pycnometer (ULTRAPYC 1200e, Quantachrome Instruments, Boynton Beach, FL, USA), and the bulk densities ( $\rho_b$ ) by a test tube. The porosity of the

particle bed ( $\varepsilon$ ) was determined by Equation 1 using  $\rho_b$  ( $\text{kg}\cdot\text{m}^{-3}$ ) and  $\rho_r$  ( $\text{kg}\cdot\text{m}^{-3}$ ), and the moisture ( $Ubu$ ), ashes' contents ( $C_Z$ ), volatile material ( $Mv$ ), and fixed carbon ( $CF$ ), were determined using AOAC [29] and ASTM [30–32] methodologies.

$$\varepsilon = 1 - \frac{\rho_b}{\rho_r} \quad (1)$$

BET (Brunauer—Emmet—Teller) and BJH (Barret—Joyner—Halenda) were used to obtain the physical structure characteristics of the activated carbons (Quantachrome Instrument, NOVA 4200e, USA). The values for the yield ( $Y$ ) of the activated carbons were obtained using Equation (2), where  $m_i$  and  $m_f$  correspond to the initial and final adsorbent mass (g), respectively.

$$Y(\%) = \frac{m_f}{m_i} 100 \quad (2)$$

X-ray diffraction (XRD, Rigaku ULTIMA IV, Tokyo, Japan) was performed to infer the crystalline structures by scanning step over the range of  $10\text{--}70^\circ$  using Bragg-Brentano geometry. The crystallinity index ( $I_c$ ) was calculated according to Equation (3) [33], where  $I_{cr}$  is the intensity of the crystalline peak and  $I_{am}$  is the intensity of the amorphous phase.

$$I_C = \frac{I_{cr} - I_{am}}{I_{cr}} 100 \quad (3)$$

The thermogravimetric analysis (TGA, Shimadzu, model TGA 50, Tokyo, Japan) was performed in  $\text{N}_2$  gas.

## 2.2. Adsorption Experiments

The molecular structural model of the MB dye is shown in Figure 2. The MB solution ( $25\text{--}1000 \text{ mg L}^{-1}$ ) was added to a  $4\text{--}20 \text{ g L}^{-1}$  of adsorbent dosage, the operating range conditions that were obtained from preliminary trials. The mixtures of adsorbent-adsorbate were agitated in a shaker (NOVA ÉTICA, model 109-1) at 120 rpm, between 1 and 120 min. The samples were centrifuged for 15 min to separate the adsorbents from the MB solution. The MB solution was quantified at a maximum wavelength of 660 nm. The capacity of adsorption and removal efficiency were calculated using Equations (4) and (5), respectively.

$$Q = \frac{C_i - C_f}{M} V \quad (4)$$

$$E = \frac{C_i - C_f}{C_i} 100 \quad (5)$$

where  $C_i$  is the initial concentration ( $\text{mg L}^{-1}$ );  $C_f$ , the final concentration ( $\text{mg L}^{-1}$ );  $M$ , the mass of adsorbent (g); and  $V$ , the volume of solution (L).

The pseudo-first-order [34], pseudo-second-order [35], and Avrami [36] models were used to analyze the kinetic data. The expressions of the models were shown in Equations (6)–(8), respectively.

$$q_t = q_e \left( 1 - e^{-k_1 t} \right) \quad (6)$$

$$q_t = \frac{k_2 q_e^2 t}{1 + k_2 q_e t} \quad (7)$$

$$q_t = q_e \left( 1 - e^{(-k_{av} t)^{n_{av}}} \right) \quad (8)$$

where  $q_t$  and  $q_e$  is the quantity of adsorbate in the adsorbent ( $\text{mg g}^{-1}$ );  $t$  is the time of contact (min);  $k_1$  is the pseudo-first-order constant ( $\text{min}^{-1}$ );  $k_2$  is the pseudo-second-order

constant ( $\text{g mg}^{-1} \text{min}^{-1}$ );  $K_{id}$  is the intra-particle constant ( $\text{g mg}^{-1} \text{min}^{-1/2}$ );  $K_{av}$  ( $1 \text{min}^{-1}$ ) and  $n_{av}$  are the Avrami constants; and  $C$  is related to diffusion resistance ( $\text{mg g}^{-1}$ ).

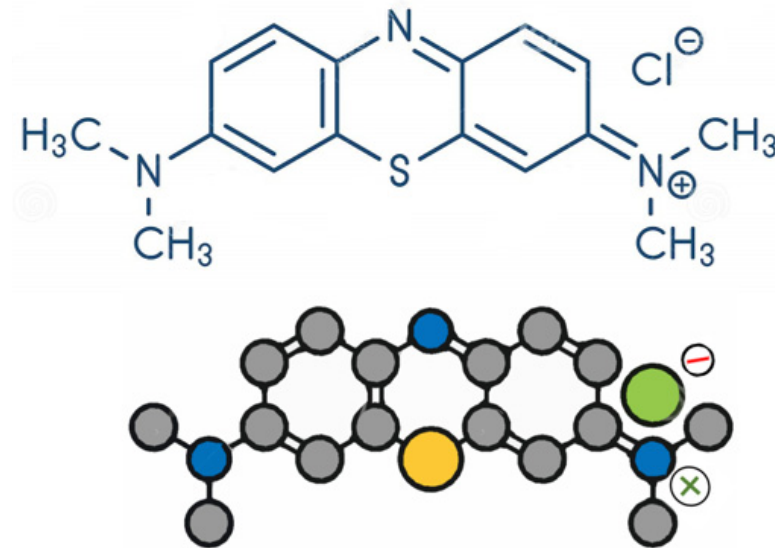


**Figure 2.** Molecular structure of methylene blue.

The data of equilibrium isotherms were fitted to the mathematical models Langmuir [37], Freundlich [38], Sips [39], and Tóth [40], presented in Equations (9)–(12).

$$q_e = \frac{q_{max} K_L C_e}{1 + K_L C_e} \quad (9)$$

$$q_e = K_F C_e^{\frac{1}{n}} \quad (10)$$

$$q_e = \frac{q_{max} (K_S C_e)^m}{1 + (K_S C_e)^m} \quad (11)$$

$$q_e = \frac{q_{max} b C_e}{(1 + (b C_e)^d)^{\frac{1}{d}}} \quad (12)$$

where  $q_e$  is the amount of MB in the adsorbent at equilibrium ( $\text{mg g}^{-1}$ );  $q_{max}$  is the maximum MB adsorbed per unit mass of the adsorbent ( $\text{mg g}^{-1}$ );  $K_L$  is the Langmuir constant of the rate of adsorption ( $\text{K mg}^{-1}$ );  $K_F$  is the Freundlich constant [ $(\text{mg L}^{-1}) (\text{mg L}^{-1})^{-1/n}$ ];  $K_S$  is the constant of Sips model ( $\text{L mg}^{-1}$ );  $b$  is the constant of Tóth model ( $\text{mg L}^{-1}$ ); and  $m$ ,  $n$ , and  $d$  are the parameters characterizing the system heterogeneity.

The analysis of the variance (ANOVA) was evaluated for all the models and the statistical values were studied at a level of confidence of 95% for each adjustment.

All the theoretical model parameters were defined through nonlinear regression using the quasi-Newton method. The models were checked by using the Chi-square ( $X^2$ ) and average relative error (ARE) according to Equations (13) and (14), respectively.

$$ARE = \frac{100}{nn} \sum \frac{q_{exp} - q_{pred}}{q_{exp}} \quad (13)$$

$$X^2 = \sum \frac{(q_{exp} - q_{pred})^2}{nn - NN} \quad (14)$$

where  $q_{exp}$  are the experimental values;  $q_{pred}$  is the value of the model;  $nn$  is the experiment number observed; and  $NN$  is the number of the parameters in the model.

### 3. Results

#### 3.1. Characterization of *Lolium multiflorum* and Adsorbents

The results of the physical characterizations of the LM, R-40, R-70, AC-40, and AC-70 samples are shown in Figure 3. The values of  $d_{ps}$  for the R-40 and R-70 were smaller than the LM, suggesting the dehydration of the raw material and structure changes after the chemical treatment. Furthermore, the AC-70 exhibits higher  $\rho_r$  than the R-70, which indicates the formation of pores, resulting from the effective thermal activation of the material. Both ACs showed Ubu lower than 5%, which is in accordance with the commercial activated carbons [41]. Thus, the increase in Cz can be attributed to the presence of inorganics after the chemical and thermal activation [42,43].

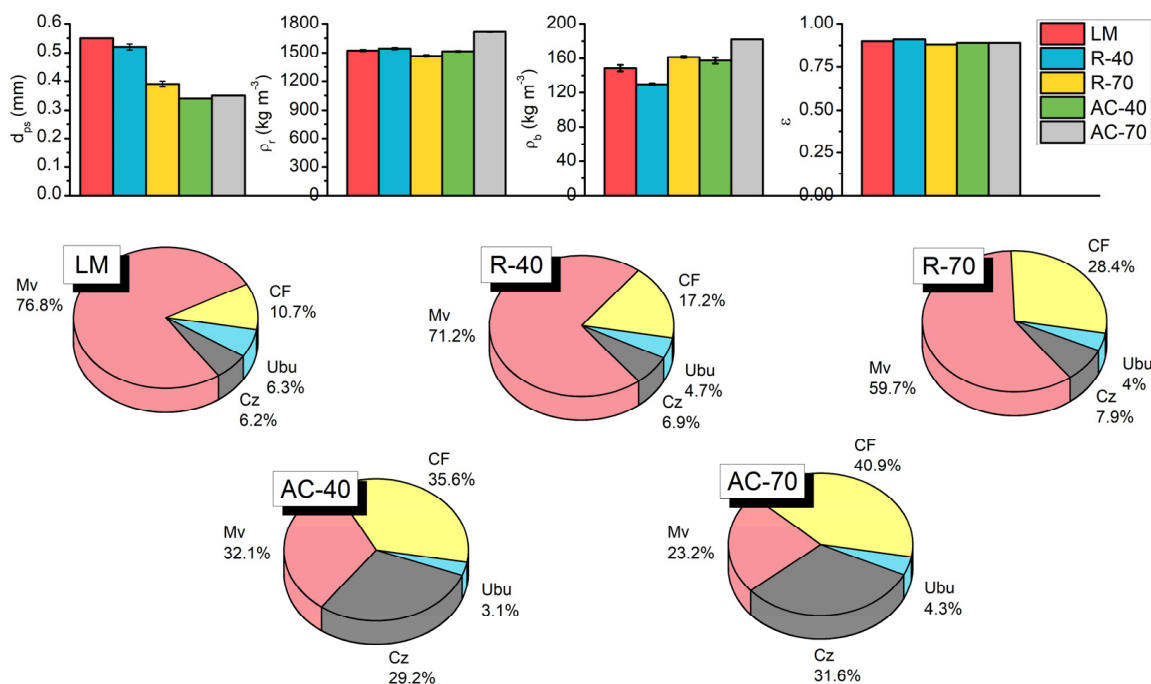


**Figure 3.** Physical characterization of LM, R-40, R-70, AC-40, and AC-70.

The R-40 and R-70 samples presented lower values of Mv than the LM, which might be attributed to the degradation caused by the  $H_3PO_4$  activation [43]. After pyrolysis, the AC-40 and AC-70 presented another decrease in Mv values and an increase in CF, indicating the carbonization of volatile materials [44], which is in agreement with the physical characteristics obtained for activated carbons (Table 1).

**Table 1.** Textural characteristics and yield of AC-40 and AC-70.

Adsorbents	$S_{BET}$ (m <sup>2</sup> g <sup>-1</sup> )	$P_V$ (cm <sup>3</sup> g <sup>-1</sup> )	$P_D$ (nm)	Y (%)
AC-40	14.50	0.0252	3.73	47.60
AC-70	68.28	0.0603	3.25	50.33

Figure 4a, b shows the TGA profiles of the LM, R-40, R-70, AC-40, and AC-70. All samples display a weight loss for the temperatures inferior to 100 °C related to the evaporation of moisture [45]. The LM sample presented a weight loss of 63% in the range between 235 and 370 °C, which is related to the degradation of hemicellulose (235–315 °C), cellulose (315–370 °C), and lignin (100–900 °C) [46]. This result agrees with the DTG peak at 278 °C and 330 °C. In the profile of the R-40 and R-70, the decomposition of cellulose was noticed in the range between 257 and 350 °C. Moreover, the less pronounced peak of cellulose and the absence of a hemicellulose shoulder in the DTG curves suggests that the chemical treatment with  $H_3PO_4$  catalyzes the hydrolysis of glucose bonds [47,48].



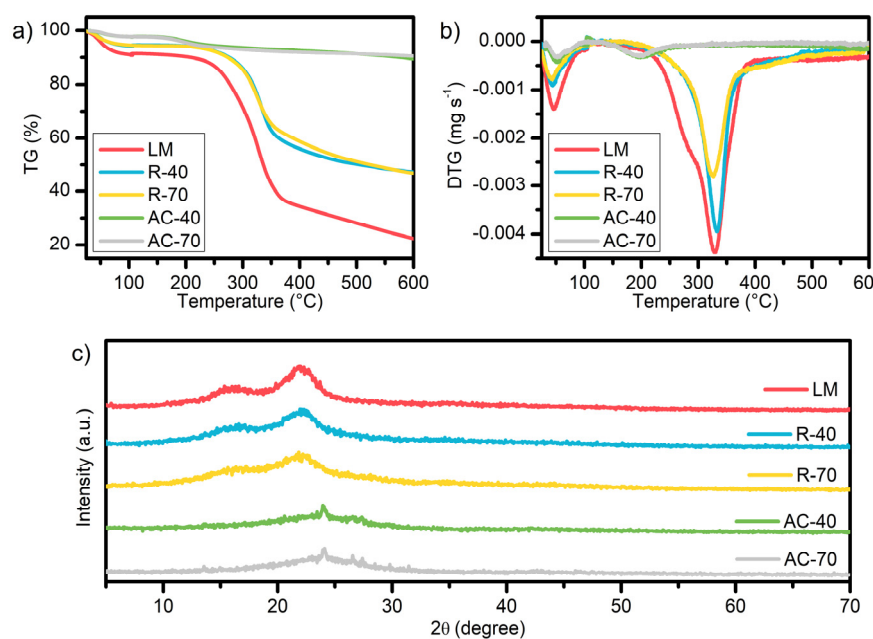


**Figure 4.** TG (a), DTG (b), and XRD (c) of LM, R-40, R-70, AC-40, and AC-70.

The weight loss of 6.6% at 197 °C for the AC-40 and AC-70 can be assigned to the volatiles related to  $H_3PO_4$  chemical activation [49]. The absence of lignin and hemicellulose peaks in the DTG, associated with the superior thermal stability of the ACs, confirms the efficiency of pyrolysis in the production of adsorbent materials.

The XRD patterns of the LM, R-40, R-70, AC-40, and AC-70 are shown in Figure 4c. The values of the crystallinity index were 39.70% and 35.43% for the R-40 and R-70, respectively. The LM showed a crystallinity index of 48.70%. The crystallinity reduction of the R-40 and R-70 can be attributed to the chemical reaction involving cellulose, since the acid diffuses into the internal and external layers of the fiber, providing the breakdown of the intramolecular and intermolecular bonds with the phosphate groups [50].

The XRD patterns of the R-40 and R-70 indicate the presence of cellulose in the peaks around 10–25 °C. This decrease in the R-40 and R-70 in relation to the LM is due to the breaking of the crystalline chains and the widening of the amorphous structure, converting the crystalline cellulose into amorphous cellulose. The non-appearance of the crystallinity of cellulose in the AC-40 and AC-70 can be assigned to the reduction in the stretching hydrogen bonds and their disorganization as an amorphous structure after the pyrolysis [50]. The AC-40 and AC-70 have a predominantly amorphous structure despite presenting a peak at 26°, which indicates a crystallinity of  $SiO_2$  [51,52]. The increase in the amorphous structure of the AC-40 and AC-70 shows that pyrolysis was effective in carbonizing the R-40 and R-70, causing a disorder in the crystalline structure and consequently creating empty spaces for the adsorption of the MB dye [53].

Figure 5 shows the FTIR spectrum of the adsorbents R-40 (a), R-70 (b), AC-40 (c), and AC-70 (d). All samples have similar absorption bands, related to the lignocellulosic constituents. In general, these bands are expected since they are often found in agricultural residues that are composed of hemicellulose, lignin, cellulose, proteins, hydrocarbons, lipids, simple sugars, and amide [54]. The band at approximately 3000–3700  $cm^{-1}$  is attributed to the stretching of O-H bonds (phenols, alcohols, and carboxylic acids) and the stretching of the -NH amine groups of the lignin [55]. The two bands at 2913–2923 and 2849  $cm^{-1}$  are related to the symmetric and asymmetric stretching of the -CH<sub>3</sub> and -CH<sub>2</sub> groups or the -C-OH group [56,57]. In both activated carbons, there was a decrease in the intensity of these peaks, suggesting a lower amount of these groups on the surface compared to the treated samples. The band around 1717  $cm^{-1}$  is characteristic of the C=O stretching of the esters, ketones, and carboxylic groups of the hemicellulose and lignin [56,58–60] followed by the C=C bond stretching in aromatic rings around 1637  $cm^{-1}$  [56]. The intense

absorption band at  $1060\text{ cm}^{-1}$  is attributed to the C-O-C of the  $\beta$ -glycosidic linkages stretch of the lignocellulosic compounds [58,61]. The peaks around  $610\text{ cm}^{-1}$  corresponds to the C-H group of the aliphatic and aromatic or the C-N groups [62–64]. In general, all the bands were more intense in the sample treated with acid at the lower concentration. This suggests that the higher concentration of the phosphoric acid used in the treatments causes a change in the groups present on the surface of the adsorbents that are visualized by the displacement of some absorption bands in the activated carbons.

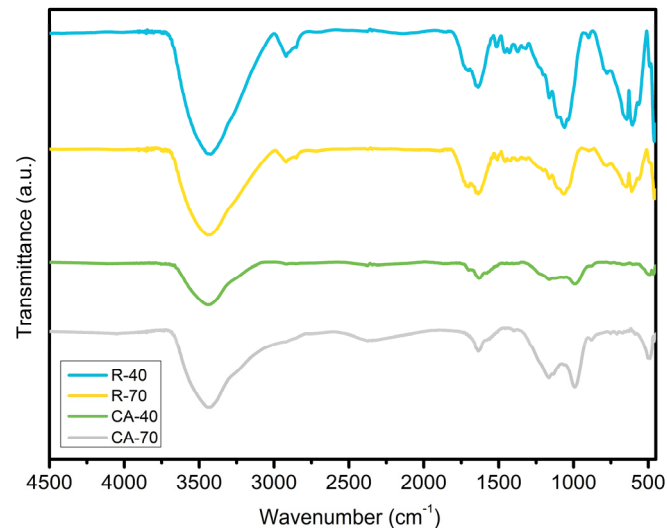


**Figure 5.** FTIR spectra of R-40, R-70, AC-40, and AC-70.

The morphology of the samples was investigated by SEM and Figure 6 shows the images of the R-40, R-70, AC-40, and AC-70 adsorbents at  $200\times$  magnification. It is observed that there is a degradation of the fibrous structures caused by the acid and a significant difference between the treated samples and the activated carbons. Among the treated samples, the R-70 showed the appearance of cavities, which were intensified by the pyrolysis process. The sample AC-70 presented a rougher surface with irregularities in the structure. It is also noticed that there is a decrease in the particle size of the sample when comparing the treated samples with the produced activated carbons.

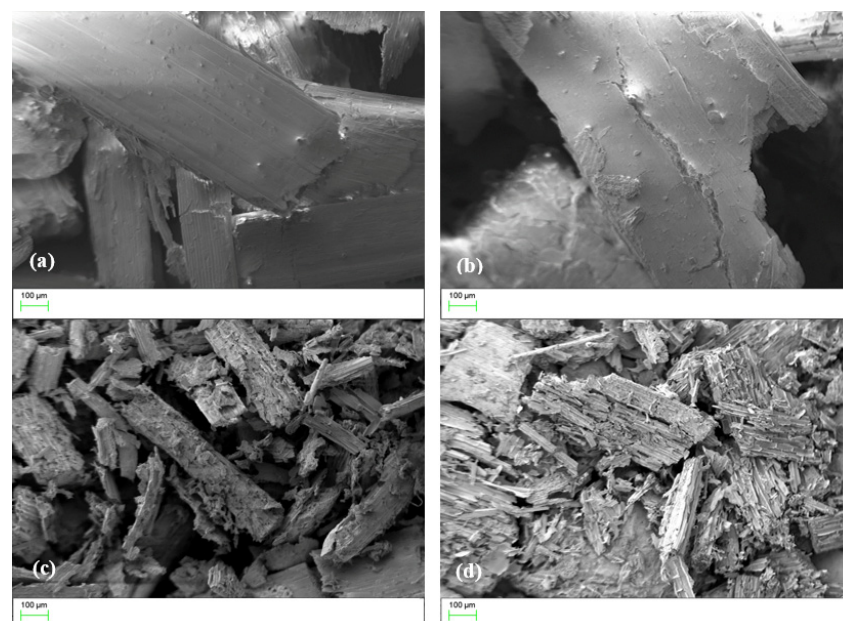


**Figure 6.** Morphology of R-40 (a), R-70 (b), AC-40 (c), and AC-70 (d).

Table 1 shows the textural characteristics of the activated carbons. The increase in surface area ( $S_{BET}$ ) and pore volume ( $P_v$ ) of the AC-70 suggests the efficiency of  $H_3PO_4$  activation and pyrolysis [43,65]. The pore diameter ( $P_D$ ) values obtained for the AC-40 and AC-70 were 3.73 nm and 3.25 nm, respectively, which implies that both adsorbents can be applied in the removal of the MB molecule ( $0.59 \times 1.38$  nm) [49,66]. The high yield percentage ( $Y$ ) of the AC-40 and AC-70 is related to the creation of phosphate film, which can protect the internal carbon structure, preventing the material from being excessively carbonized and limiting the formation of tar during pyrolysis [46].

### 3.2. Adsorption Experiments

The kinetic adjustment of the experimental data was obtained for the Pseudo-first-order, Pseudo-second-order, and Avrami models. The faster adsorption was detected in the first moments of contact between the adsorbents and the MB molecules (Figure 7). A rapid adsorption is an important feature of adsorbents for practical application in wastewater treatment [67,68]. The kinetic results indicate that the increase of contact time between the solid and liquid phases increases MB adsorption. The R-40, R-70, AC-40, and AC-70 reached the equilibrium in 2, 5, 20, and 10 min, respectively. The increase in the equilibrium time for the activated carbon can be attributed to structural characteristics, such as the average pore diameter after pyrolysis. The mass transfer in the pores of the adsorbents is generally controlled by their size [67]; i.e., the larger the pore size, the smaller the contribution of resistance to the intraparticle diffusion in the control of adsorption kinetics [67]. Table S1 shows the parameters obtained through the application of the kinetic models for the experimental data.

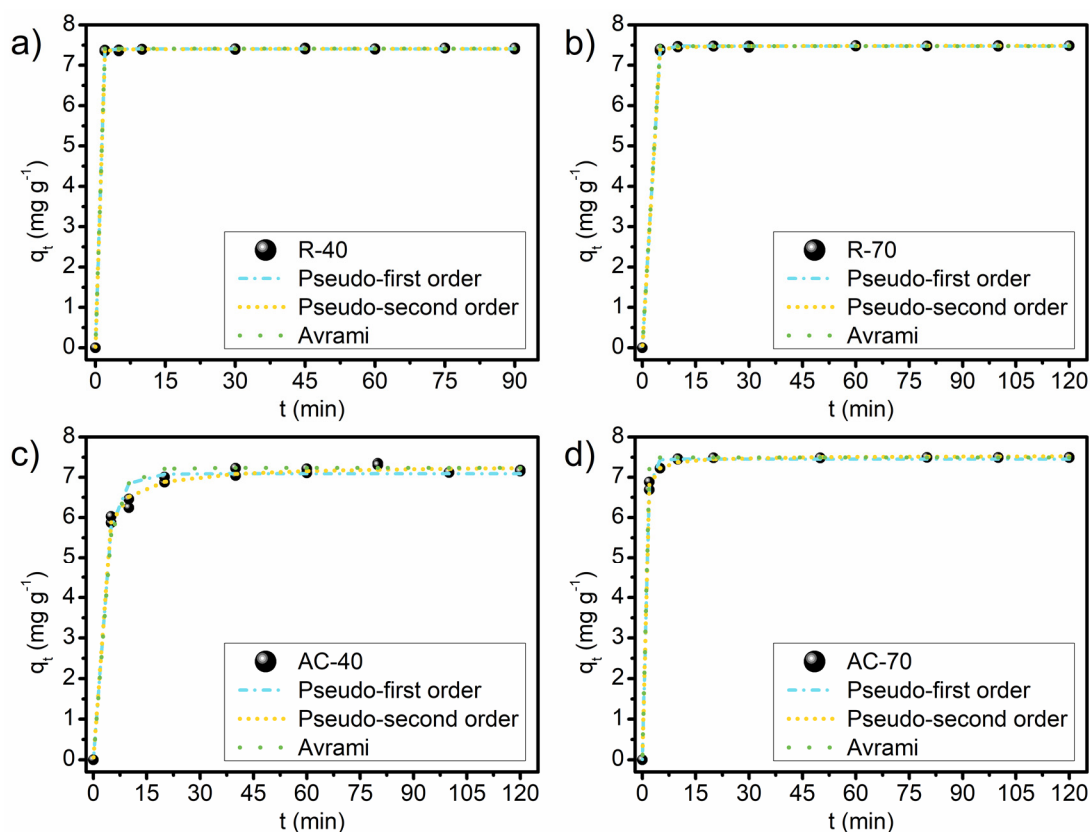


**Figure 7.** Kinetic curves of adsorption of MB on R-40 (a), R-70 (b), AC-40 (c), and AC-70 (d). Conditions:  $C_0$ ,  $150 \text{ mg L}^{-1}$ ; temperature,  $25 \text{ }^\circ\text{C}$ ; adsorbent dosage,  $20 \text{ g L}^{-1}$ ; pH, unaltered.

Pseudo-first-order, Pseudo-second-order, and Avrami models showed higher correlation coefficients ( $R^2$ ) and lower values for  $ARE$  and  $X^2$  for all adsorbents. The Pseudo-first-order model indicates that the adsorption of MB occurs predominantly through physical



mechanisms [69,70]. The empty sites are proportional to the occupancy rate of the adsorption sites [71].

The Pseudo-second-order model suggests that electrons are shared or exchanged between the surface of the adsorbents and the MB molecules [72]. This indicates that the interaction of the surface of the R-40, R-70, AC-40, and AC-70 with the MB molecules occurs due to the delocalized electrons on the basal planes of the adsorbent and the free electrons of the aromatic rings of the MB molecules [73]. In this study, the Avrami model is adequate to describe all the kinetic experimental data, assuming multiple kinetic orders during the process. The Avrami exponent ( $n$ ) is a fractional number related to the possible changes in the adsorption mechanism during the process [74]. The adsorption mechanism could follow multiple kinetic orders that are changed during the adsorption process [75]. A better interpretation of the adsorption mechanisms can be obtained in the plots of  $q_t$  versus  $t^{1/2}$  (Figure 8). All the adsorbents showed a multilinearity of the lines. This implies that the adsorption process involves more than one kinetic stage, which is in agreement with the good fit obtained with the Avrami kinetic model [72,76]. The R-40 and R-70 exhibited two stages: the first can be attributed to instant adsorption, with the mass transfer of the dye to the surface of the adsorbent particles [77]; the second stage can be defined as the final stage of equilibrium. For these adsorbents, it is observed that the resistance to intraparticle diffusion is practically non-existent and the dye is adsorbed on the external surface. The AC-40 and AC-70 showed three stages of kinetic mechanisms: external adsorption, gradual diffusion within the pores, and the equilibrium stage. In the equilibrium stage, the diffusion within the particles decreases due to extremely low concentrations (less than  $3 \text{ mg L}^{-1}$ ) of the adsorbate in the solution [75,76,78].

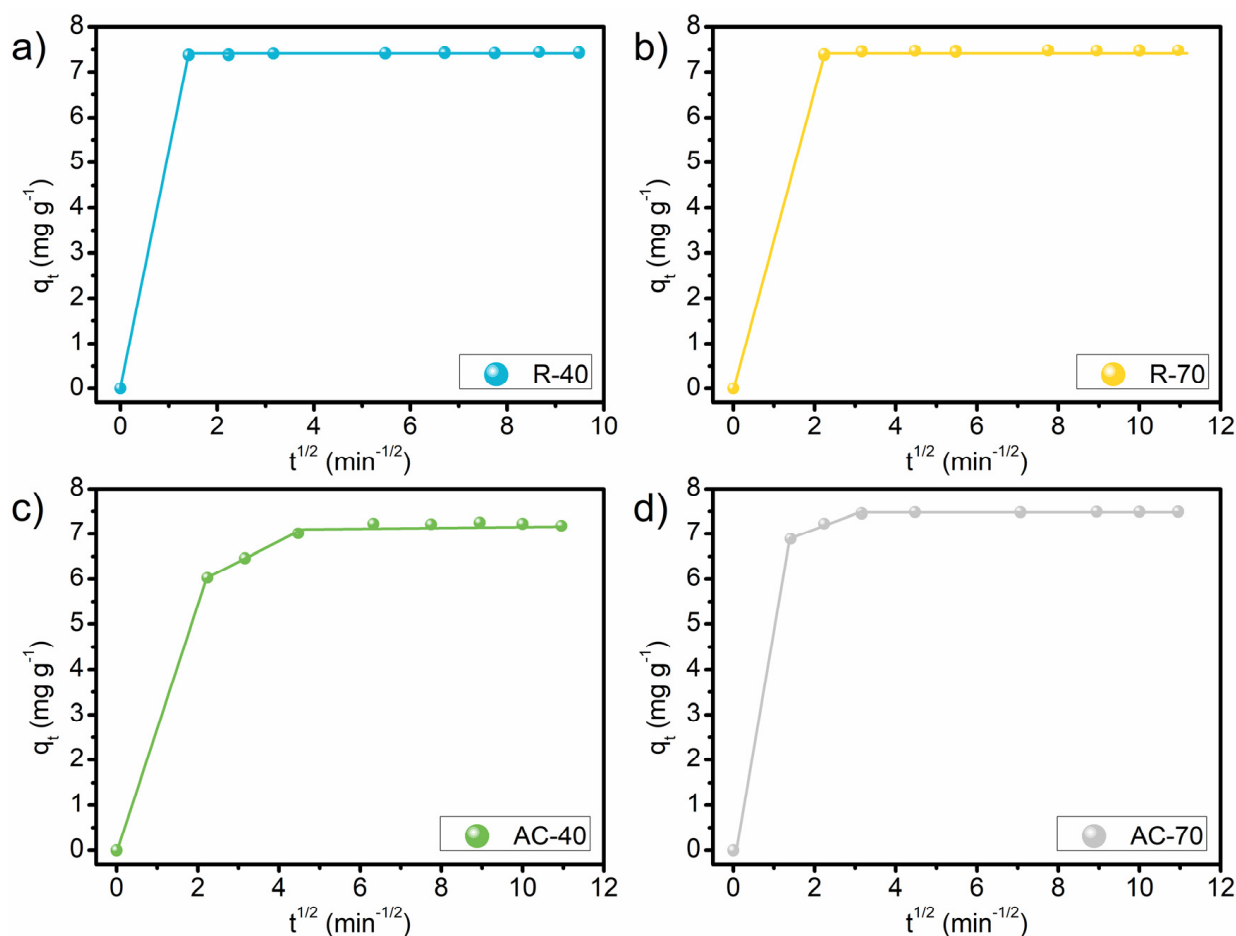


**Figure 8.** Linear plot of kinetics of MB onto R-40 (a), R-70 (b), AC-40 (c), and AC-70 (d). Conditions: Co,  $150 \text{ mg L}^{-1}$ ; temperature,  $25 \text{ }^\circ\text{C}$ ; adsorbent dosage,  $20 \text{ g L}^{-1}$ ; pH, unaltered.

The results of the adsorption equilibrium data of the MB dye for the R-40, R-70, AC-40, and AC-70 at 25 °C are shown in Figure 9, and the adjustments of Langmuir, Freundlich, Sips, and Tóth models are presented in Table S2. The shape of the equilibrium curves indicates a favorable adsorption process from all adsorbents; i.e., the increase of the adsorption capacity and the increase of the adsorbate concentration are proportionate. This behavior occurs when the adsorbent-adsorbate interaction has a great affinity [28,69]. The profile of the curve of the AC-40 and R-40 can be also classified as a Langmuir type (L) [79]. The L type initially tends to curve downwards due to a decrease in the availability of active sites, indicating that the molecules are adsorbed on the surface of the adsorbent. For the AC-70 and R-70, the shape of the curve can be classified as a High-affinity type (H) due to an initial vertical part of the isotherm curve, suggesting that adsorption is high even at low initial MB concentrations.

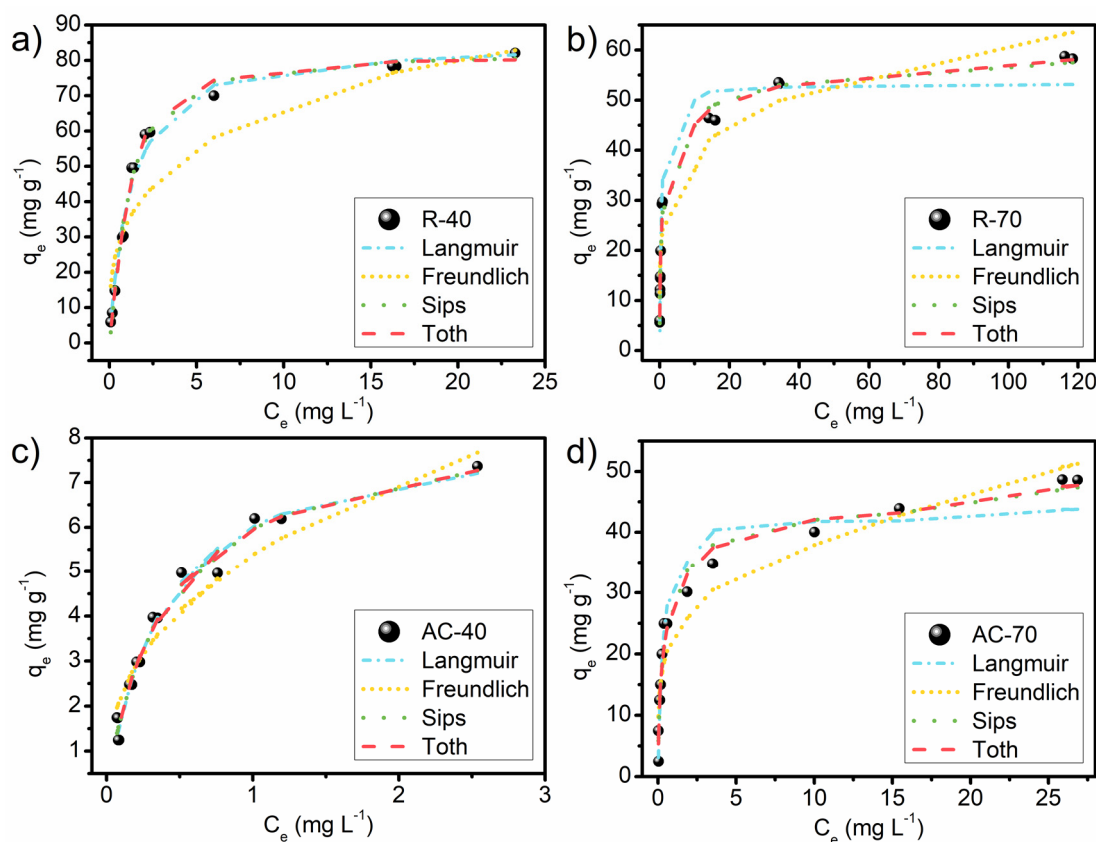


**Figure 9.** Isothermal curves of adsorption of MB on R-40 (a), R-70 (b), AC-40 (c), and AC-70 (d) at 25 °C. Conditions: adsorbent dosage, 4 g L<sup>-1</sup> for R-40 and R-70 and 20 g L<sup>-1</sup> for AC-40 and AC-70; pH, unaltered; contact time, 60 min.

Table S2 describes that the best adjustment of the experimental data occurred with the Tóth model for all the adsorbent materials. This is verified by the highest values of  $R^2$  and lowest values of  $X^2$  and  $ARE$ . The  $d$  values being close to one for the R-40 and AC-40 indicate that MB adsorption is highly homogeneous [80]. For the R-70 and AC-70, the  $d$  values were not close to one, implying a heterogeneous adsorption [81]. This can be explained by the larger amount of H<sub>3</sub>PO<sub>4</sub> used in the samples of the R-70 and AC-70. The  $b$  values obtained for the R-70 and AC-70 were 20.96 and 7.55, higher than the R-40 ( $b = 0.60$ ) and AC-40 ( $b = 2.85$ ), which indicates a better affinity with the MB molecules. Regarding the  $b$  values obtained in the literature from the MB adsorption, it is worth mentioning the zeolite 13× [80]; the activated carbon from Delonix regia [74]; and the zeolite from rice husk ash [82] that obtained 0.93, 0.06, and 0.47 respectively. This corroborates the interpretation of the high affinity between the MB molecules and the adsorbents produced from the LM.

The AC-40, AC-70, and R-70 also presented significant adjustments with the Sips model and the  $m$  values ( $m < 1$ ), demonstrating the increase of heterogeneity from the R-70 and AC-70, in agreement with the  $d$  values obtained by the Tóth model. Concerning the AC-40, aside from having the adjustments mentioned above, the great fit of the Langmuir model suggests that it can also be used to describe its adsorption process in accordance with the  $d$  values. This model proposes that the MB dye molecules form an adsorbate monolayer on the material surface, filling the pores [67,72,83]. In most cases, more than one model can explain the adsorption process [84].

Table 2 shows a comparison of the  $q_{max}$  values of the adsorption of the MB dye for the adsorbents obtained in this work with the values similar studies reported. The values of  $q_{max}$  for the R-40, R-70, AC-70, and AC-40 were 80.79 mg g<sup>-1</sup>, 70.21 mg g<sup>-1</sup>, 53.32 mg g<sup>-1</sup>, and 8.2 mg g<sup>-1</sup>, respectively. For all adsorbents, the dye removal efficiency was about 99%. These results suggest that the LM was efficient in MB wastewater treatment. Moreover, these results are in agreement with the previous study where the LM activated with NaOH obtained a  $q_{max}$  of 67.19 mg g<sup>-1</sup>, compared to the 28.8 mg g<sup>-1</sup> for the LM without treatment [28]. The higher  $q_{max}$  for the LM adsorbent activated with H<sub>3</sub>PO<sub>4</sub> agrees with other reports, as can be seen in Table 2.

**Table 2.** Comparison of different adsorbents for removal of MB dye.

Adsorbents from Biomass	Chemical Activation	C <sub>0</sub> (mg L <sup>-1</sup> )	Temperature (°C)	Contact Time (h)	$m_{ads}/V_{sol}$ (g L <sup>-1</sup> )	pH	$q_{max}$ (mg g <sup>-1</sup> )
R-40	H <sub>3</sub> PO <sub>4</sub>	25–360	25	2	4	7	80.79
R-70	H <sub>3</sub> PO <sub>4</sub>	25–360	25	2	4	7	70.21
AC-40	H <sub>3</sub> PO <sub>4</sub>	25–150	25	2	20	7	8.20
AC-70	H <sub>3</sub> PO <sub>4</sub>	50–1000	25	2	20	7	53.32
LM [28]	-	150	-	2	4–32	7	28.70
LM + NaOH [28]	NaOH	150	-	1	4–32	-	67.19
Carica papaya wood [85]	-	10–50	-	2.3	2	10	32.25
Coconut shell [86]	H <sub>2</sub> SO <sub>4</sub>	25–200	30	3	1	8	50.60
AC—Corncob [87]	H <sub>3</sub> PO <sub>4</sub>	300–1500	-	5	2	-	112.00
Mango seedkernel poder [88]	H <sub>2</sub> SO <sub>4</sub>	100	30	0.5	4	8	58.08
Mucuna beans [89]	HCl + HNO <sub>3</sub>	100	25	-	5	5	19.28
Mucuna beans [89]	NaOH	100	25	-	5	7,8	19.93
Orange tree sawdust [90]	NaOH	40–100	20	3	1	6	78.74
<i>Parthenium hysterophorus</i> [91]	H <sub>3</sub> PO <sub>4</sub>	50–250	26	1.5	4	7	88.49
<i>Parthenium hysterophorus</i> [91]	H <sub>2</sub> SO <sub>4</sub>	50–250	26	1.5	4	7	39.68
Seed husk of Timbaúva [92]	-	10–50	25	-	20	-	3.62
Sugarcane Bagasse [93]	-	10–50	30	1.5	1.5	6	1.83
Waste fruits of <i>Rapanea ferruginea</i> [8]	H <sub>2</sub> SO <sub>4</sub>	20–120	25	2	1.2	7	33.00
AC- waste of sunflower oil [94]	H <sub>2</sub> SO <sub>4</sub>	0–250	25	24	2	6	16.43
AC- Coconut fiber [95]	ZnCl <sub>2</sub>	60–100	30	1.6	5	8	15.49
AC- Apricot stones [96]	H <sub>3</sub> PO <sub>4</sub> + HNO <sub>3</sub>	5–100	25	2	0.1	5	36.68

AC = Activated Carbon.

Moreover, the lower values of  $q_{max}$  obtained for the AC-40 and AC-70 may be related to the carbon pores not being completely unobstructed and being less accessible than the surfaces of the R-40 and R-70. This result indicates a substantial increase in the adsorption of MB when the LM was treated with H<sub>3</sub>PO<sub>4</sub>. The highest value of the maximum capacity of adsorption in this work was reached with the R-40 sample, confirming that even in smaller percentages H<sub>3</sub>PO<sub>4</sub> is efficient for the chemical activation of the LM. It is important to mention that the non-use of pyrolysis in the production process of the LM adsorbent reduces energy costs, and, consequently, financial costs. The adsorbent R-40 proved to be an excellent low-cost adsorbent for removing the MB dye in aqueous solutions, in addition to being a great option for using LM straw agricultural waste.

### 3.3. Adsorption Mechanism

The adsorption process is very complex and can involve more than one mechanism. For this mechanism, it is important to understand the basic principles of the adsorption process [97]. Figure 10 suggests the mechanisms that may be involved in the adsorption

of MB using treated ryegrass straw (R-40, R-70) and activated carbons (AC-40, AC-70). In Figure 10, the possible interactions that occur between the MB molecules (cationic dye) and the adsorbents produced can be observed. Three types of interactions are proposed: electrostatic,  $\pi$ - $\pi$  bonds, and interactions with the functional groups present on the surface of the adsorbents [56,98]. Electrostatic interactions can occur with the attraction between the cations of the MB and the surface of the adsorbent when the adsorbent has a negative charge. This is one of the main mechanisms reported for the adsorption of MB by bioadsorbents [99,100].  $\pi$ - $\pi$  interactions can occur due to the presence of the aromatic rings of lignin in the structures of the adsorbents and MB.

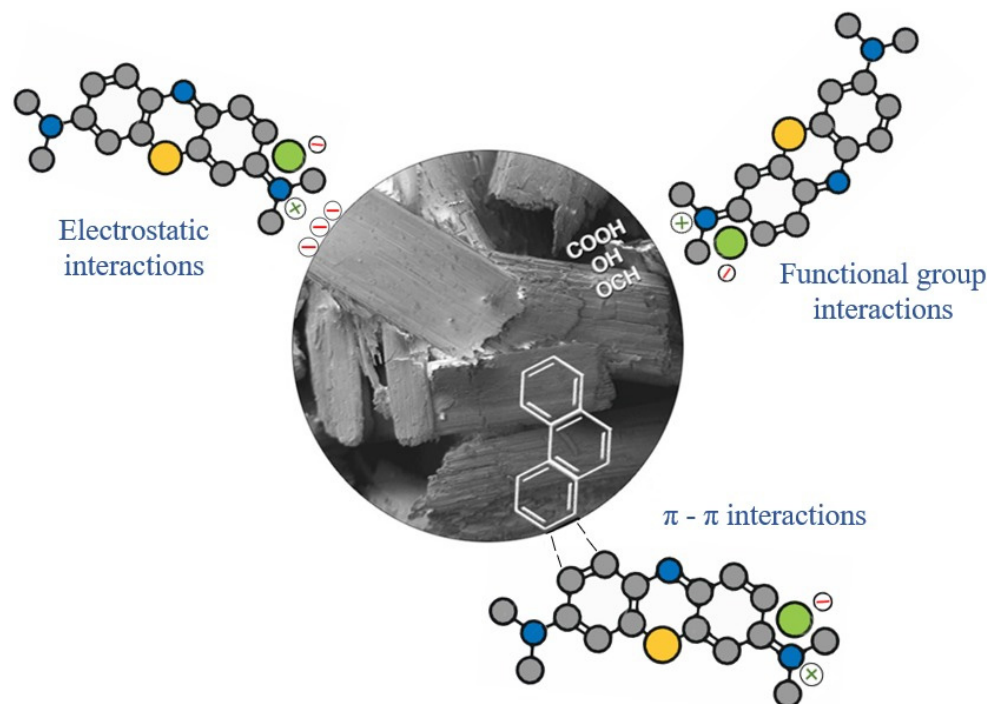


**Figure 10.** Suggestion for the mechanism of MB dye adsorption.

From the FTIR analysis, some functional groups present in the adsorbents (-OH, -COOH, C=O, -OCH<sub>3</sub>) were found to be derived from the main biomass component (cellulose, hemicellulose, and lignin). These groups may have interacted with hydrogen bonds as well as Van der Waals forces [56,100]. Among the functional groups, it was observed that the adsorbent with the highest amount of OH groups on the surface (R-40) showed the best adsorption capacity of the MB dye. This suggests that the predominant mechanism in this study was the interaction between the functional groups. The OH group interaction has already been observed in other studies. Cusioli et al. [100] reported the interaction of the OH group by hydrogen bonding between the aromatic N of MB and the H of the hydroxyl group for the adsorption of MB on soybean hulls. Al-Ghouti and Sweleh [98] and Manna et al. [101] stated that both hydrogen bonds, mainly those involving -OH groups, and electrostatic interactions play an important role in the MB adsorption by lignocellulosic materials.

#### 4. Conclusions

The H<sub>3</sub>PO<sub>4</sub> was efficient in the chemical activation of the LM straw, causing the degradation of hemicellulose and cellulose. Pyrolysis was effective in the production of activated carbons, producing the AC-40 and AC-70 with a predominantly amorphous structure and with a  $S_{BET}$  of 14.5 m<sup>2</sup> g<sup>-1</sup> and 68.2 m<sup>2</sup> g<sup>-1</sup>, respectively. All the adsorbents have a good interaction with the MB molecule, reaching the equilibrium time in less than 20 min and with a removal efficiency of about 99%. The best kinetic adjustment for the adsorption of the MB dye was obtained from the Avrami model, showing that the kinetic

experimental data assumes multiple kinetic orders during the adsorption process. The Tóth model showed the best isotherm adjustment for all the adsorbents produced. Chemical activation with 40% H<sub>3</sub>PO<sub>4</sub> in the LM straw showed the highest adsorption capacity (80.79 mg g<sup>-1</sup>) of the MB dye. The good and fast performances of the materials produced in this work suggests that ryegrass is an excellent precursor for the adsorbent materials to be applied in the treatment of colored effluents contaminated with MB.

**Supplementary Materials:** The following supporting information can be downloaded at: <https://www.mdpi.com/article/10.3390/c9020044/s1>, Table S1: Kinetic parameters of adsorption of MB on R-40, R-70, AC-40, and AC-70. Conditions: Co, 150 mg L<sup>-1</sup>; temperature, 25 °C; adsorbent dosage, 20 g L<sup>-1</sup> pH, unaltered; Table S2: Isothermal parameters of adsorption of MB on R-40, R-70, AC-40, and AC-70 at 25 °C. Conditions: adsorbent dosage, 4 g L<sup>-1</sup> for R-40 and R-70, and 20 g L<sup>-1</sup> for AC-40 and AC-70; pH, unaltered; contact time, 60 min.

**Author Contributions:** E.O.d.S.: Conceptualization; methodology; investigation; formal analysis; visualization; writing—original draft; A.V.F.: Writing of the review and editing; visualization; administration of the paper; E.B.d.A., T.D.A. and M.C.d.S.: Methodology: formal analysis; R.Z.: Paper review; G.S.d.R.: Writing of the review and editing; A.R.F.d.A.: Conceptualization; methodology; writing of the review and editing. All authors have read and agreed to the published version of the manuscript.

**Funding:** This research was funded by Coordenação de Aperfeiçoamento de Pessoal de Nível Superior (CAPES), grant number 001.

**Institutional Review Board Statement:** Not applicable.

**Informed Consent Statement:** Not applicable.

**Data Availability Statement:** Not applicable.

**Acknowledgments:** The authors would like to thank the support from National Council for Scientific and Technological Development (CNPq), Coordination for the Improvement of Higher Education Personnel (CAPES) and Foundation for Research Support of the State of Rio Grande do Sul (FAPERGS).

**Conflicts of Interest:** The authors declare no conflict of interest.

## References

1. Ali, I.; Aboul-Enein, H.Y. *Instrumental Methods in Metal Ion Speciation*; CRC Press: Boca Raton, FL, USA, 2006; ISBN 9780429133350.
2. dos Santos, K.J.L.; de Souza dos Santos, G.E.; de Sá, Í.M.G.L.; de Carvalho, S.H.V.; Soletti, J.I.; Meili, L.; da Silva Duarte, J.L.; Bispo, M.D.; Dotto, G.L. Syagrus Oleracea-Activated Carbon Prepared by Vacuum Pyrolysis for Methylene Blue Adsorption. *Environ. Sci. Pollut. Res.* **2019**, *26*, 16470–16481. [[CrossRef](#)] [[PubMed](#)]
3. Rajendran, S.; Khan, M.M.; Gracia, F.; Qin, J.; Gupta, V.K.; Arumainathan, S. Ce<sup>3+</sup>-Ion-Induced Visible-Light Photocatalytic Degradation and Electrochemical Activity of ZnO/CeO<sub>2</sub> Nanocomposite. *Sci. Rep.* **2016**, *6*, 31641. [[CrossRef](#)] [[PubMed](#)]
4. El-Zawahry, M.M.; Abdelghaffar, F.; Abdelghaffar, R.A.; Hassabo, A.G. Equilibrium and Kinetic Models on the Adsorption of Reactive Black 5 from Aqueous Solution Using Eichhornia Crassipes/Chitosan Composite. *Carbohydr. Polym.* **2016**, *136*, 507–515. [[CrossRef](#)] [[PubMed](#)]
5. Holkar, C.R.; Jadhav, A.J.; Pinjari, D.V.; Mahamuni, N.M.; Pandit, A.B. A Critical Review on Textile Wastewater Treatments: Possible Approaches. *J. Environ. Manag.* **2016**, *182*, 351–366. [[CrossRef](#)]
6. Zaini, M.A.A.; Zakaria, M.; Mohd.-Setapar, S.H.; Che-Yunus, M.A. Sludge-Adsorbents from Palm Oil Mill Effluent for Methylene Blue Removal. *J. Environ. Chem. Eng.* **2013**, *1*, 1091–1098. [[CrossRef](#)]
7. Gobi, K.; Mashitah, M.D.; Vadivelu, V.M. Adsorptive Removal of Methylene Blue Using Novel Adsorbent from Palm Oil Mill Effluent Waste Activated Sludge: Equilibrium, Thermodynamics and Kinetic Studies. *Chem. Eng. J.* **2011**, *171*, 1246–1252. [[CrossRef](#)]
8. Chahm, T.; Martins, B.A.; Rodrigues, C.A. Adsorption of Methylene Blue and Crystal Violet on Low-Cost Adsorbent: Waste Fruits of Rapanea Ferruginea (Ethanol-Treated and H<sub>2</sub>SO<sub>4</sub>-Treated). *Environ. Earth Sci.* **2018**, *77*, 508. [[CrossRef](#)]
9. Li, Z.; Hanafy, H.; Zhang, L.; Sellaoui, L.; Schadeck Netto, M.; Oliveira, M.L.S.; Seliem, M.K.; Luiz Dotto, G.; Bonilla-Petriciolet, A.; Li, Q. Adsorption of Congo Red and Methylene Blue Dyes on an Ashitaba Waste and a Walnut Shell-Based Activated Carbon from Aqueous Solutions: Experiments, Characterization and Physical Interpretations. *Chem. Eng. J.* **2020**, *388*, 124263. [[CrossRef](#)]
10. Mahmoud, D.K.; Salleh, M.A.M.; Karim, W.A.W.A.; Idris, A.; Abidin, Z.Z. Batch Adsorption of Basic Dye Using Acid Treated Kenaf Fibre Char: Equilibrium, Kinetic and Thermodynamic Studies. *Chem. Eng. J.* **2012**, *181–182*, 449–457. [[CrossRef](#)]



11. Ghaedi, M.; Heidarpour, S.; Nasiri Kokhdan, S.; Sahraie, R.; Daneshfar, A.; Brazesh, B. Comparison of Silver and Palladium Nanoparticles Loaded on Activated Carbon for Efficient Removal of Methylene Blue: Kinetic and Isotherm Study of Removal Process. *Powder Technol.* **2012**, *228*, 18–25. [[CrossRef](#)]
12. Rafatullah, M.; Sulaiman, O.; Hashim, R.; Ahmad, A. Adsorption of Methylene Blue on Low-Cost Adsorbents: A Review. *J. Hazard. Mater.* **2010**, *177*, 70–80. [[CrossRef](#)] [[PubMed](#)]
13. Wawrzkievicz, M.; Wiśniewska, M.; Wołowicz, A.; Gun'ko, V.M.; Zarko, V.I. Mixed Silica-Alumina Oxide as Sorbent for Dyes and Metal Ions Removal from Aqueous Solutions and Wastewaters. *Microporous Mesoporous Mater.* **2017**, *250*, 128–147. [[CrossRef](#)]
14. Dotto, L.G.; Salau, N.P.G.; Picin, J.S.; Cadaval, T.R.S., Jr.; De Pinto, L.A.A. *Adsorption Processes for Water Treatment and Purification*; Bonilla-Petriciolet, A., Mendoza-Castillo, D.I., Reynel-Ávila, H.E., Eds.; Springer International Publishing: Cham, Switzerland, 2017; p. 256.
15. Pourhakkak, P.; Taghizadeh, A.; Taghizadeh, M.; Ghaedi, M.; Haghdoost, S. Fundamentals of Adsorption Technology. In *Interface Science and Technology*; Mehrorang Ghaedi, Ed.; Elsevier: Amsterdam, The Netherlands, 2021; pp. 1–70.
16. Shahmoradi Ghaheh, F.; Taghizadeh, M.; Taghizadeh, A.; Hayati, B.; Mahmoodi, N.M.; Parastar, S. Clean Synthesis of Rock Candy-like Metal–Organic Framework Biocomposite for Toxic Contaminants Remediation. *Environ. Technol. Innov.* **2021**, *23*, 101747. [[CrossRef](#)]
17. Wamba, A.G.N.; Ndi, S.K.; Lima, E.C.; Kayem, J.G.; Thue, P.S.; Costa, T.M.H.; Quevedo, A.B.; Benvenuti, E.V.; Machado, F.M. Preparation, Characterization of Titanate Nanosheet–Pozzolan Nanocomposite and Its Use as an Adsorbent for Removal of Diclofenac from Simulated Hospital Effluents. *J. Taiwan Inst. Chem. Eng.* **2019**, *102*, 321–329. [[CrossRef](#)]
18. Liew, R.K.; Chai, C.; Yek, P.N.Y.; Phang, X.Y.; Chong, M.Y.; Nam, W.L.; Su, M.H.; Lam, W.H.; Ma, N.L.; Lam, S.S. Innovative Production of Highly Porous Carbon for Industrial Effluent Remediation via Microwave Vacuum Pyrolysis plus Sodium–Potassium Hydroxide Mixture Activation. *J. Clean. Prod.* **2019**, *208*, 1436–1445. [[CrossRef](#)]
19. Fan, S.; Wang, Y.; Wang, Z.; Tang, J.; Tang, J.; Li, X. Removal of Methylene Blue from Aqueous Solution by Sewage Sludge-Derived Biochar: Adsorption Kinetics, Equilibrium, Thermodynamics and Mechanism. *J. Environ. Chem. Eng.* **2017**, *5*, 601–611. [[CrossRef](#)]
20. Seid-Mohammadi, A.; Asgarai, G.; Ghorbanian, Z.; Dargahi, A. The Removal of Cephalexin Antibiotic in Aqueous Solutions by Ultrasonic Waves/Hydrogen Peroxide/Nickel Oxide Nanoparticles (US/H<sub>2</sub>O<sub>2</sub>/NiO) Hybrid Process. *Sep. Sci. Technol.* **2020**, *55*, 1558–1568. [[CrossRef](#)]
21. Asuha, S.; Fei, F.; Wurendaodi, W.; Zhao, S.; Wu, H.; Zhuang, X. Activation of Kaolinite by a Low-Temperature Chemical Method and Its Effect on Methylene Blue Adsorption. *Powder Technol.* **2020**, *361*, 624–632. [[CrossRef](#)]
22. Ren, C.; Guo, D.; Liu, X.; Li, R.; Zhang, Z. Performance of the Emerging Biochar on the Stabilization of Potentially Toxic Metals in Smelter- and Mining-Contaminated Soils. *Environ. Sci. Pollut. Res.* **2020**, *27*, 43428–43438. [[CrossRef](#)]
23. Imran, M.; Islam, A.; Farooq, M.U.; Ye, J.; Zhang, P. Characterization and Adsorption Capacity of Modified 3D Porous Aerogel from Grapefruit Peels for Removal of Oils and Organic Solvents. *Environ. Sci. Pollut. Res.* **2020**, *27*, 43493–43504. [[CrossRef](#)]
24. Park, M.H.; Jeong, S.; Kim, J.Y. Adsorption of NH<sub>3</sub>-N onto Rice Straw-Derived Biochar. *J. Environ. Chem. Eng.* **2019**, *7*, 103039. [[CrossRef](#)]
25. Rovani, S.; Rodrigues, A.G.; Medeiros, L.F.; Cataluña, R.; Lima, É.C.; Fernandes, A.N. Synthesis and Characterisation of Activated Carbon from Agroindustrial Waste—Preliminary Study of 17β-Estradiol Removal from Aqueous Solution. *J. Environ. Chem. Eng.* **2016**, *4*, 2128–2137. [[CrossRef](#)]
26. Ma, Y. Comparison of Activated Carbons Prepared from Wheat Straw via ZnCl<sub>2</sub> and KOH Activation. *Waste Biomass Valorization* **2017**, *8*, 549–559. [[CrossRef](#)]
27. Fontaneli, R.S.; Santos, H.P.; Fontaneli, R.S. *FORAGEIRAS PARA INTEGRAÇÃO LAVOURA-PECUÁRIA-FLORESTA NA REGIÃO SUL-BRASILEIRA*, 2nd ed.; Renato Serena Fontaneli, H.P., dos Santos, R.S.F., Eds.; Embrapa: Brasília, Brazil, 2012; ISBN 9788570351043.
28. Silva, E.O.; Santos, V.D.; Araujo, E.B.; Guterres, F.P.; Zottis, R.; Flores, W.H.; Almeida, A.R.F. Removal of Methylene Blue from Aqueous Solution by Ryegrass Straw. *Int. J. Environ. Sci. Technol.* **2020**, *17*, 3723–3740. [[CrossRef](#)]
29. Cunniff, P.; AOAC International. *Official Methods of Analysis of AOAC International*, 18th ed.; AOAC International: Gaithersburg, MD, USA, 1997.
30. ASTM International. *ASTM D 1762-84: Standard Test Method for Chemical Analysis of Wood Charcoal*; ASTM International: West Conshohocken, PA, USA, 2013.
31. ASTM International. *ASTM E872-82: Standard Test Method for Volatile Matter in the Analysis of Particulate Wood Fuels*; ASTM International: West Conshohocken, PA, USA, 2013.
32. ASTM International. *ASTM E1755: Standard Test Method for Ash in Biomass*; ASTM International: West Conshohocken, PA, USA, 2015.
33. Segal, L.; Creely, J.J.; Martin, A.E.; Conrad, C.M. An Empirical Method for Estimating the Degree of Crystallinity of Native Cellulose Using the X-Ray Diffractometer. *Text. Res. J.* **1959**, *29*, 786–794. [[CrossRef](#)]
34. Lagergren, S.Y. Zur Theorie Der Sogenannten Adsorption Gelöster Stoffe. *Z. Für Chem. Und Ind. Kolloide* **1907**, *2*, 15. [[CrossRef](#)]
35. Ho, Y.; McKay, G. Pseudo-Second Order Model for Sorption Processes. *Process Biochem.* **1999**, *34*, 451–465. [[CrossRef](#)]
36. Lopes, E.C.N.; Dos Anjos, F.S.C.; Vieira, E.F.S.; Cestari, A.R. An Alternative Avrami Equation to Evaluate Kinetic Parameters of the Interaction of Hg(II) with Thin Chitosan Membranes. *J. Colloid Interface Sci.* **2003**, *263*, 542–547. [[CrossRef](#)]
37. Langmuir, I. The Adsorption of Gases on Plane Surfaces of Glass, Mica and Platinum. *J. Am. Chem. Soc.* **1918**, *40*, 1361–1403. [[CrossRef](#)]
38. Freundlich, H.M.F. Over the Adsorption in Solution. *J. Phys. Chem.* **1906**, *57*, 385–471.

39. Sips, R. On the Structure of a Catalyst Surface. *J. Chem. Phys.* **1948**, *16*, 490–495. [[CrossRef](#)]
40. Tóth, J. State Equations of the Solid-Gas Interface Layers. *Acta Chim. (Acad. Sci. Hung.)* **1971**, *69*, 311–328.
41. Silgado, K.J.; Marrugo, G.D.; Puello, J. Adsorption of Chromium (VI) by Activated Carbon Produced from Oil Palm Endocarp. *Chem. Eng. Trans.* **2014**, *37*, 721–726. [[CrossRef](#)]
42. Puchana-Rosero, M.J.; Adebayo, M.A.; Lima, E.C.; Machado, F.M.; Thue, P.S.; Vaghetti, J.C.P.; Umpierrez, C.S.; Gutterres, M. Microwave-Assisted Activated Carbon Obtained from the Sludge of Tannery-Treatment Effluent Plant for Removal of Leather Dyes. *Colloids Surf. A Physicochem. Eng. Asp.* **2016**, *504*, 105–115. [[CrossRef](#)]
43. Anisuzzaman, S.M.; Joseph, C.G.; Daud, W.M.A.B.W.; Krishnaiah, D.; Yee, H.S. Preparation and Characterization of Activated Carbon from Typha Orientalis Leaves. *Int. J. Ind. Chem.* **2015**, *6*, 9–21. [[CrossRef](#)]
44. Boonamnuyvitaya, V.; Sae-Ung, S.; Tanthapanichakoon, W. Preparation of Activated Carbons from Coffee Residue for the Adsorption of Formaldehyde. *Sep. Purif. Technol.* **2005**, *42*, 159–168. [[CrossRef](#)]
45. Valério Filho, A.; Xavaré Kulman, R.; Vaz Tholozan, L.; Felkl de Almeida, A.R.; Silveira da Rosa, G. Preparation and Characterization of Activated Carbon Obtained from Water Treatment Plant Sludge for Removal of Cationic Dye from Wastewater. *Processes* **2020**, *8*, 1549. [[CrossRef](#)]
46. Rosas, J.M.; Bedia, J.; Rodríguez-Mirasol, J.; Cordero, T. HEMP-Derived Activated Carbon Fibers by Chemical Activation with Phosphoric Acid. *Fuel* **2009**, *88*, 19–26. [[CrossRef](#)]
47. Bansal, P.; Hall, M.; Realff, M.J.; Lee, J.H.; Bommarius, A.S. Multivariate Statistical Analysis of X-Ray Data from Cellulose: A New Method to Determine Degree of Crystallinity and Predict Hydrolysis Rates. *Bioresour. Technol.* **2010**, *101*, 4461–4471. [[CrossRef](#)]
48. Wassie, A.B.; Srivastava, V.C. Chemical Treatment of Teff Straw by Sodium Hydroxide, Phosphoric Acid and Zinc Chloride: Adsorptive Removal of Chromium. *Int. J. Environ. Sci. Technol.* **2016**, *13*, 2415–2426. [[CrossRef](#)]
49. Filho, A.V.; Kulman, R.X.; Janner, N.N.; Tholozan, L.V.; de Almeida, A.R.F.; da Rosa, G.S. Optimization of Cationic Dye Removal Using a High Surface Area-Activated Carbon from Water Treatment Sludge. *Bull. Mater. Sci.* **2021**, *44*, 41. [[CrossRef](#)]
50. Gao, C.; Xiong, G.Y.; Luo, H.L.; Ren, K.J.; Huang, Y.; Wan, Y.Z. Dynamic Interaction between the Growing Ca-P Minerals and Bacterial Cellulose Nanofibers during Early Biomineralization Process. *Cellulose* **2010**, *17*, 365–373. [[CrossRef](#)]
51. Ferreira, C.S.; Santos, P.L.; Bonacin, J.A.; Passos, R.R.; Pocrifka, L.A. Rice Husk Reuse in the Preparation of SnO<sub>2</sub>/SiO<sub>2</sub> Nanocomposite. *Mater. Res.* **2015**, *18*, 639–643. [[CrossRef](#)]
52. Zuo, R.F.; Du, G.X.; Yang, W.G.; Liao, L.B.; Li, Z. Mineralogical and Chemical Characteristics of a Powder and Purified Quartz from Yunnan Province. *Open Geosci.* **2016**, *8*, 606–611. [[CrossRef](#)]
53. Lima, D.R.; Sellaoui, L.; Klein, L.; Reis, G.S.; Lima, É.C.; Dotto, G.L. Physicochemical and Thermodynamic Study of Malachite Green Adsorption on Raw and Modified Corn Straw. *Can. J. Chem. Eng.* **2018**, *96*, 779–787. [[CrossRef](#)]
54. Valério Filho, A.; Tholozan, L.V.; da Silva, E.O.; Meili, L.; de Almeida, A.R.F.; da Rosa, G.S. Perspectives of the Reuse of Agricultural Wastes from the Rio Grande Do Sul, Brazil, as New Adsorbent Materials. In *Biomass-Derived Materials for Environmental Applications*; Anastopoulos, I., Lima, E.C., Meili, L., Giannakoudakis, D.A., Eds.; Elsevier: Amsterdam, The Netherlands, 2022; pp. 243–266. ISBN 9780323919142.
55. Raupp, Í.N.; Valério Filho, A.; Arim, A.L.; Muniz, A.R.C.; da Rosa, G.S. Development and Characterization of Activated Carbon from Olive Pomace: Experimental Design, Kinetic and Equilibrium Studies in Nimesulide Adsorption. *Materials* **2021**, *14*, 6820. [[CrossRef](#)]
56. Bortoluz, J.; Ferrarini, F.; Bonetto, L.R.; da Silva Crespo, J.; Giovanela, M. Use of Low-Cost Natural Waste from the Furniture Industry for the Removal of Methylene Blue by Adsorption: Isotherms, Kinetics and Thermodynamics. *Cellulose* **2020**, *27*, 6445–6466. [[CrossRef](#)]
57. Tholozan, L.V.; Valério Filho, A.; Maron, G.K.; Carreno, N.L.V.; da Rocha, C.M.; Bordin, J.; da Rosa, G.S. Sphagnum Perichaetiale Hampe Biomass as a Novel, Green, and Low-Cost Biosorbent in the Adsorption of Toxic Crystal Violet Dye. *Environ. Sci. Pollut. Res.* **2023**, *30*, 52472–52484. [[CrossRef](#)]
58. Filho, A.C.D.; Mazzocato, A.C.; Dotto, G.L.; Thue, P.S.; Pavan, F.A. Eragrostis Plana Nees as a Novel Eco-Friendly Adsorbent for Removal of Crystal Violet from Aqueous Solutions. *Environ. Sci. Pollut. Res.* **2017**, *24*, 19909–19919. [[CrossRef](#)]
59. Pang, X.; Sellaoui, L.; Franco, D.; Netto, M.S.; Georgin, J.; Luiz Dotto, G.; Abu Shayeb, M.K.; Belmabrouk, H.; Bonilla-Petriciolet, A.; Li, Z. Preparation and Characterization of a Novel Mountain Soursop Seeds Powder Adsorbent and Its Application for the Removal of Crystal Violet and Methylene Blue from Aqueous Solutions. *Chem. Eng. J.* **2020**, *391*, 123617. [[CrossRef](#)]
60. Cimirro, N.F.G.M.; Lima, E.C.; Cunha, M.R.; Dias, S.L.P.; Thue, P.S.; Mazzocato, A.C.; Dotto, G.L.; Gelesky, M.A.; Pavan, F.A. Removal of Pharmaceutical Compounds from Aqueous Solution by Novel Activated Carbon Synthesized from Lovegrass (Poaceae). *Environ. Sci. Pollut. Res.* **2020**, *27*, 21442–21454. [[CrossRef](#)] [[PubMed](#)]
61. Salomón, Y.L.O.; Georgin, J.; Franco, D.S.P.; Netto, M.S.; Foletto, E.L.; Allasia, D.; Dotto, G.L. Application of Seed Residues from Anadenanthera Macrocarpa and Cedrela Fissilis as Alternative Adsorbents for Remarkable Removal of Methylene Blue Dye in Aqueous Solutions. *Environ. Sci. Pollut. Res.* **2021**, *28*, 2342–2354. [[CrossRef](#)]
62. Franco, D.S.P.; Fagundes, J.L.S.; Georgin, J.; Salau, N.P.G.; Dotto, G.L. A Mass Transfer Study Considering Intraparticle Diffusion and Axial Dispersion for Fixed-Bed Adsorption of Crystal Violet on Pecan Pericarp (*Carya Illinoensis*). *Chem. Eng. J.* **2020**, *397*, 125423. [[CrossRef](#)]

63. Salomón, Y.L.D.O.; Georgin, J.; Reis, G.; Lima, E.C.; Oliveira, M.L.S.; Franco, D.S.P.; Netto, M.S.; Allasia, D.; Dotto, G.L. Utilization of Pacara Earpod Tree (*Enterolobium Contortisilquum*) and Ironwood (*Caesalpinia Leiostachya*) Seeds as Low-Cost Biosorbents for Removal of Basic Fuchsin. *Environ. Sci. Pollut. Res.* **2020**, *27*, 33307–33320. [[CrossRef](#)] [[PubMed](#)]
64. Salomón, Y.L.D.O.; Georgin, J.; Franco, D.S.; Netto, M.S.; Piccilli, D.G.; Foletto, E.L.; Oliveira, L.F.; Dotto, G.L. High-Performance Removal of 2,4-Dichlorophenoxyacetic Acid Herbicide in Water Using Activated Carbon Derived from Queen Palm Fruit Endocarp (*Syagrus Romanzoffiana*). *J. Environ. Chem. Eng.* **2021**, *9*, 104911. [[CrossRef](#)]
65. Yacob, A.R.; Al Swaidan, H.M. Phosphoric Acid Effect on Prepared Activated Carbon from Saudi Arabia's Date Frond Waste. *Appl. Mech. Mater.* **2012**, *110–116*, 2124–2130. [[CrossRef](#)]
66. Macedo, J.D.S.; Júnior, N.B.D.C.; Almeida, L.E.; Vieira, E.F.D.S.; Cestari, A.R.; Gimenez, I.D.F.; Carreño, N.L.V.; Barreto, L.S. Kinetic and Calorimetric Study of the Adsorption of Dyes on Mesoporous Activated Carbon Prepared from Coconut Coir Dust. *J. Colloid Interface Sci.* **2006**, *298*, 515–522. [[CrossRef](#)]
67. Fontana, K.B.; Chaves, E.S.; Sanchez, J.D.S.; Watanabe, E.R.L.R.; Pietrobelli, J.M.T.A.; Lenzi, G.G. Textile Dye Removal from Aqueous Solutions by Malt Bagasse: Isotherm, Kinetic and Thermodynamic Studies. *Ecotoxicol. Environ. Saf.* **2016**, *124*, 329–336. [[CrossRef](#)]
68. Li, H.; Dong, X.; da Silva, E.B.; de Oliveira, L.M.; Chen, Y.; Ma, L.Q. Mechanisms of Metal Sorption by Biochars: Biochar Characteristics and Modifications. *Chemosphere* **2017**, *178*, 466–478. [[CrossRef](#)]
69. Alves, C.C.O.; Franca, A.S.; Oliveira, L.S. Comparison of Microwave Assisted Thermo-Chemical Procedures in the Production of Adsorbents for Wastewater Treatment. *Int. J. Environ. Sci. Dev.* **2015**, *6*, 888–894. [[CrossRef](#)]
70. Xie, X.; Gao, H.; Luo, X.; Su, T.; Zhang, Y.; Qin, Z. Polyethyleneimine Modified Activated Carbon for Adsorption of Cd(II) in Aqueous Solution. *J. Environ. Chem. Eng.* **2019**, *7*, 103183. [[CrossRef](#)]
71. Kumar, P.; Chauhan, M.S. Adsorption of Chromium (VI) from the Synthetic Aqueous Solution Using Chemically Modified Dried Water Hyacinth Roots. *J. Environ. Chem. Eng.* **2019**, *7*, 103218. [[CrossRef](#)]
72. Valério Filho, A.; Tholozan, L.V.; Arim, A.L.; de Almeida, A.R.F.; da Rosa, G.S. High-Performance Removal of Anti-Inflammatory Using Activated Carbon from Water Treatment Plant Sludge: Fixed-Bed and Batch Studies. *Int. J. Environ. Sci. Technol.* **2023**, *20*, 3633–3644. [[CrossRef](#)]
73. Archin, S.; Sharifi, S.H.; Asadpour, G. Optimization and Modeling of Simultaneous Ultrasound-Assisted Adsorption of Binary Dyes Using Activated Carbon from Tobacco Residues: Response Surface Methodology. *J. Clean. Prod.* **2019**, *239*, 118136. [[CrossRef](#)]
74. Vargas, A.M.M.; Cazetta, A.L.; Kunita, M.H.; Silva, T.L.; Almeida, V.C. Adsorption of Methylene Blue on Activated Carbon Produced from Flamboyant Pods (*Delonix Regia*): Study of Adsorption Isotherms and Kinetic Models. *Chem. Eng. J.* **2011**, *168*, 722–730. [[CrossRef](#)]
75. Vagheti, J.C.P.; Lima, E.C.; Royer, B.; da Cunha, B.M.; Cardoso, N.F.; Brasil, J.L.; Dias, S.L.P. Pecan Nutshell as Biosorbent to Remove Cu(II), Mn(II) and Pb(II) from Aqueous Solutions. *J. Hazard. Mater.* **2009**, *162*, 270–280. [[CrossRef](#)]
76. Calvete, T.; Lima, E.C.; Cardoso, N.F.; Vagheti, J.C.P.; Dias, S.L.P.; Pavan, F.A. Application of Carbon Adsorbents Prepared from Brazilian-Pine Fruit Shell for the Removal of Reactive Orange 16 from Aqueous Solution: Kinetic, Equilibrium, and Thermodynamic Studies. *J. Environ. Manag.* **2010**, *91*, 1695–1706. [[CrossRef](#)] [[PubMed](#)]
77. Alves, C.C.O.; Franca, A.S.; Oliveira, L.S. Removal of Phenylalanine from Aqueous Solutions with Thermo-Chemically Modified Corn Cobs as Adsorbents. *LWT-Food Sci. Technol.* **2013**, *51*, 1–8. [[CrossRef](#)]
78. dos Reis, G.S.; Adebayo, M.A.; Sampaio, C.H.; Lima, E.C.; Thue, P.S.; de Brum, I.A.S.; Dias, S.L.P.; Pavan, F.A. Removal of Phenolic Compounds from Aqueous Solutions Using Sludge-Based Activated Carbons Prepared by Conventional Heating and Microwave-Assisted Pyrolysis. *Water Air Soil Pollut.* **2017**, *228*, 33. [[CrossRef](#)]
79. Giles, C.H.; MacEwan, T.H.; Nakhwa, S.N.; Smith, D. Studies in Adsorption. Part XI. A System of Classification of Solution Adsorption Isotherms, and Its Use in Diagnosis of Adsorption Mechanisms and in Measurement of Specific Surface Areas of Solids. *J. Chem. Soc.* **1960**, *846*, 3973. [[CrossRef](#)]
80. Amiri, M.K.; Ghaemi, A.; Arjomandi, H. Experimental, Kinetics and Isothermal Modeling of Carbon Dioxide Adsorption with 13X Zeolite in a Fixed Bed Column. *Iran. J. Chem. Eng.* **2019**, *16*, 54–64.
81. Cazetta, A.L.; Vargas, A.M.M.; Nogami, E.M.; Kunita, M.H.; Guilherme, M.R.; Martins, A.C.; Silva, T.L.; Moraes, J.C.G.; Almeida, V.C. NaOH-Activated Carbon of High Surface Area Produced from Coconut Shell: Kinetics and Equilibrium Studies from the Methylene Blue Adsorption. *Chem. Eng. J.* **2011**, *174*, 117–125. [[CrossRef](#)]
82. Ramezani, H.; Azizi, S.N.; Cravotto, G. Improved Removal of Methylene Blue on Modified Hierarchical Zeolite Y: Achieved by a “Destructive-Constructive” Method. *Green Process. Synth.* **2019**, *8*, 730–741. [[CrossRef](#)]
83. Brion-Roby, R.; Gagnon, J.; Nosrati, S.; Deschênes, J.S.; Chabot, B. Adsorption and Desorption of Molybdenum(VI) in Contaminated Water Using a Chitosan Sorbent. *J. Water Process Eng.* **2018**, *23*, 13–19. [[CrossRef](#)]
84. Febrianto, J.; Kosasih, A.N.; Sunarso, J.; Ju, Y.H.; Indraswati, N.; Ismadi, S. Equilibrium and Kinetic Studies in Adsorption of Heavy Metals Using Biosorbent: A Summary of Recent Studies. *J. Hazard. Mater.* **2009**, *162*, 616–645. [[CrossRef](#)]
85. Rangabhashiyam, S.; Lata, S.; Balasubramanian, P. Biosorption Characteristics of Methylene Blue and Malachite Green from Simulated Wastewater onto Carica Papaya Wood Biosorbent. *Surf. Interfaces* **2018**, *10*, 197–215. [[CrossRef](#)]
86. Jawad, A.H.; Abdulhameed, A.S.; Mastuli, M.S. Acid-Fractionalized Biomass Material for Methylene Blue Dye Removal: A Comprehensive Adsorption and Mechanism Study. *J. Taibah Univ. Sci.* **2020**, *14*, 305–313. [[CrossRef](#)]

87. Sych, N.V.; Trofymenko, S.I.; Poddubnaya, O.I.; Tsyba, M.M.; Sapsay, V.I.; Klymchuk, D.O.; Puziy, A.M. Porous Structure and Surface Chemistry of Phosphoric Acid Activated Carbon from Corncob. *Appl. Surf. Sci.* **2012**, *261*, 75–82. [[CrossRef](#)]
88. Senthil Kumar, P.; Palaniyappan, M.; Priyadharshini, M.; Vignesh, A.M.; Thanjiappan, A.; Sebastina Anne Fernando, P.; Tanvir Ahmed, R.; Srinath, R. Adsorption of Basic Dye onto Raw and Surface-Modified Agricultural Waste. *Environ. Prog. Sustain. Energy* **2014**, *33*, 87–98. [[CrossRef](#)]
89. Shooto, N.D.; Thabede, P.M.; Bhila, B.; Moloto, H.; Naidoo, E.B. Lead Ions and Methylene Blue Dye Removal from Aqueous Solution by Mucuna Beans (Velvet Beans) Adsorbents. *J. Environ. Chem. Eng.* **2020**, *8*, 103557. [[CrossRef](#)]
90. Azzaz, A.A.; Jellali, S.; Akrouf, H.; Assadi, A.A.; Bousselmi, L. Optimization of a Cationic Dye Removal by a Chemically Modified Agriculture By-Product Using Response Surface Methodology: Biomasses Characterization and Adsorption Properties. *Environ. Sci. Pollut. Res.* **2017**, *24*, 9831–9846. [[CrossRef](#)]
91. Lata, H.; Garg, V.K.; Gupta, R.K. Removal of a Basic Dye from Aqueous Solution by Adsorption Using Parthenium Hysterophorus: An Agricultural Waste. *Dye. Pigment.* **2007**, *74*, 653–658. [[CrossRef](#)]
92. Lima, J.P.; Alvarenga, G.; Goszczynski, A.C.F.; Rosa, G.R.; Lopes, T.J. Batch Adsorption of Methylene Blue Dye Using Enterolobium Contortisiliquum as Bioadsorbent: Experimental, Mathematical Modeling and Simulation. *J. Ind. Eng. Chem.* **2020**, *91*, 362–371. [[CrossRef](#)]
93. Yadav, V.; Ali, J.; Garg, M.C. Biosorption of Methylene Blue Dye from Textile-Industry Wastewater onto Sugarcane Bagasse: Response Surface Modeling, Isotherms, Kinetic and Thermodynamic Modeling. *J. Hazard. Toxic Radioact. Waste* **2021**, *25*, 04020067. [[CrossRef](#)]
94. Karagöz, S.; Tay, T.; Ucar, S.; Erdem, M. Activated Carbons from Waste Biomass by Sulfuric Acid Activation and Their Use on Methylene Blue Adsorption. *Bioresour. Technol.* **2008**, *99*, 6214–6222. [[CrossRef](#)]
95. Sharma, Y.C.; Uma; Upadhyay, S.N. Removal of a Cationic Dye from Wastewaters by Adsorption on Activated Carbon Developed from Coconut Coir. *Energy Fuels* **2009**, *23*, 2983–2988. [[CrossRef](#)]
96. Djilani, C.; Zaghoudi, R.; Djazi, F.; Bouchekima, B.; Lallam, A.; Modarressi, A.; Rogalski, M. Adsorption of Dyes on Activated Carbon Prepared from Apricot Stones and Commercial Activated Carbon. *J. Taiwan Inst. Chem. Eng.* **2015**, *53*, 112–121. [[CrossRef](#)]
97. Mashkoor, F.; Nasar, A. Magnetized Tectona Grandis Sawdust as a Novel Adsorbent: Preparation, Characterization, and Utilization for the Removal of Methylene Blue from Aqueous Solution. *Cellulose* **2020**, *27*, 2613–2635. [[CrossRef](#)]
98. Al-Ghouti, M.A.; Sweleh, A.O. Optimizing Textile Dye Removal by Activated Carbon Prepared from Olive Stones. *Environ. Technol. Innov.* **2019**, *16*, 100488. [[CrossRef](#)]
99. Salazar-Rabago, J.J.; Leyva-Ramos, R.; Rivera-Utrilla, J.; Ocampo-Perez, R.; Cerino-Cordova, F.J. Biosorption Mechanism of Methylene Blue from Aqueous Solution onto White Pine (*Pinus Durangensis*) Sawdust: Effect of Operating Conditions. *Sustain. Environ. Res.* **2017**, *27*, 32–40. [[CrossRef](#)]
100. Cusioli, L.F.; Quesada, H.B.; Baptista, A.T.A.; Gomes, R.G.; Bergamasco, R. Soybean Hulls as a Low-cost Biosorbent for Removal of Methylene Blue Contaminant. *Environ. Prog. Sustain. Energy* **2020**, *39*, e13328. [[CrossRef](#)]
101. Manna, S.; Roy, D.; Saha, P.; Gopakumar, D.; Thomas, S. Rapid Methylene Blue Adsorption Using Modified Lignocellulosic Materials. *Process Saf. Environ. Prot.* **2017**, *107*, 346–356. [[CrossRef](#)]

**Disclaimer/Publisher's Note:** The statements, opinions and data contained in all publications are solely those of the individual author(s) and contributor(s) and not of MDPI and/or the editor(s). MDPI and/or the editor(s) disclaim responsibility for any injury to people or property resulting from any ideas, methods, instructions or products referred to in the content.